

Sensor Development for the CMS Pixel Detector

D. Bortoletto^{*}, V. Chiochia[‡], S. Cucciarelli^{||}, A. Dorokhov^{†‡}, M. Konecki^{||},
K. Prokofiev^{†‡}, C. Regenfus[‡], T. Rohe[¶], S. Son^{*}, T. Speer[‡], M. Swartz[§]
^{*}Purdue University, Task G, West Lafayette, IN 47907, USA

[†]Paul Scherrer Institut, Villigen, Switzerland

[‡]Physik Institut der Universität Zürich, Switzerland

^{||}Institut für Physik der Universität Basel, Switzerland

[§]Johns Hopkins University, Baltimore, Md., USA

[¶]Speaker. E-mail address: tilman.rohe@cern.ch

Abstract—This paper reports on a current R&D activity for the sensor part of the CMS pixel detector. Devices featuring several design and technology options have been irradiated up to a proton fluence¹ of $1 \times 10^{15} \text{ n}_{\text{eq}}/\text{cm}^2$ at the CERN PS. Afterwards they have been bump bonded to unirradiated readout chips. The chips allow a non zero suppressed full analogue readout and therefore a good characterization of the sensors in terms of noise and charge collection properties. The samples have been tested using high energy pions in the H2 beam line of the CERN SPS in June and September 2003. The results of this test beam are presented and the differences between the sensor options are discussed.

I. INTRODUCTION

The CMS experiment, currently under construction at the Large Hadron Collider (LHC) at CERN (Geneva, Switzerland), will contain a hybrid pixel detector for tracking and vertexing. This paper reports on the development of the sensor part of the system. A general overview on the CMS pixel project is given in ref. [1]. Because of the harsh radiation environment at the LHC the technical realization of the pixel detector is extremely challenging. All components of the pixel detector are specified to remain operational up to a particle fluence of at least $6 \times 10^{14} \text{ n}_{\text{eq}}/\text{cm}^2$.

This implies that the pixel sensors have to deliver a sufficiently high signal until the end of their life time. The final readout chips feature built-in data sparcification with a threshold set to 2000-3000 electrons in order to suppress noise hits. With a sensor thickness of $285 \mu\text{m}$ a minimum ionizing particle creates about 20 000 electron-hole pairs (most probable value). However, with increasing irradiation this charge cannot be fully collected due to trapping and incomplete depletion. As both effects can be reduced by increasing the sensor bias, the choice of the sensor concept must allow the application of elevated bias voltages without causing electrical breakdown. For the CMS pixel detector a maximum value of 500-600 V is foreseen. In addition to the radiation-induced effects there might be regions in the sensor with lower charge collection efficiency which have to be minimized by design optimization.

The aim of this study is to compare two different design and technology options for the sensor part of the CMS pixel

detector with respect to their signal collection properties.

II. SENSOR CONCEPTS UNDER STUDY

After the irradiation-induced space charge inversion of the substrate and the subsequent increase of the full depletion voltage, sensors might have to be operated partially depleted. Therefore an “*n-in-n*” concept has been chosen. In addition double sided processing of these devices allows for the implementation of guard rings on the *p*-side of the sensor only, keeping all sensor edges on ground potential. The design of the guard rings has been optimized in the past. The breakdown voltage exceeds by far the required value of about 600 V.

For readout of the ohmic *n*-side of the sensor, inter-pixel isolation has to be provided. Here *p*-stops are considered as well as the *p*-spray technique. In order to test the segmented devices on wafer with IV-measurements and to keep accidentally unconnected pixel cells close to ground potential, high resistive electrical connections between the pixels have been implemented. In the case of *p*-stops this was realized by openings in the *p*-stop implants. The properties of such “resistors” formed by the electron accumulation layer have been studied in detail in ref. [2], [3]. According to previous investigations [3], [4] the most promising geometries feature small distances between the *n*⁺-implants and quite large *p*-stop openings (see fig.1, left). These kinds of structures have been implemented in our latest prototype sensor productions delivered in 2002. Following the recommendation of the ROSE collaboration [5], oxygen enriched silicon has been used to improve the post irradiation behavior.

In addition we investigated prototypes featuring the moderated *p*-spray isolation technique. Here the isolating *p*-implant is performed without a photolithographic mask and therefore no structuring is possible. However punch-through biasing can be implemented. Its behavior is much less dependent on outer conditions like backside bias and radiation effects than the resistors formed by electron accumulation. The layout (see fig. 1, right) is characterized by small gaps of $20 \mu\text{m}$ between the *n*⁺-implants and by a minimized biasing structure using small “bias dots” [6].

¹All fluences are normalized to 1 MeV neutrons ($\text{n}_{\text{eq}}/\text{cm}^2$)

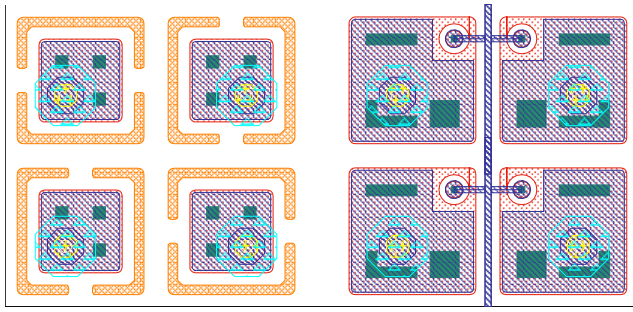


Fig. 1. Mask layout of the pixel sensors under study. Open p -stop rings (left) and p -spray with bias grid (right). Colors code: red: n^+ -implant, orange: p -stop, blue: metal, green (solid): contact between n^+ -implant and metal, yellow: passivation opening, turquoise: bump metallization.

III. TEST PROCEDURE

Several miniature sensors of the two designs with 22×32 square pixels (pitch: $125 \mu\text{m}$) were bump bonded to readout chips of the type PSI30/AC30² described in detail in ref [7]. This chip allows to force a sequential readout of all 704 pixel cells without zero suppression. All comparators are switched off by masking the pixels or setting the thresholds to very high values. The sampling time at the shaper is defined by an external hold signal. The shaping times of the preamplifier and the shaper were adjusted in a way to prevent saturation of the preamplifier and shaper up to signals corresponding to about 1 – 1.5 minimal ionizing particles. For the test beam a pin-diode was used to provide the external hold signal and to trigger the readout.

Some of the sensors were irradiated at the CERN PS in May 2003 after bump deposition but before being attached to the readout chips. The irradiation was performed at room temperature without bias. The fluences applied were 3, 8, and $11 \times 10^{14} \text{ n}_{\text{eq}}/\text{cm}^2$. In order to avoid reverse annealing the sensors were stored at -20°C after irradiation and warmed up to room temperature only for transport and bump bonding. For the irradiated sensors a special bump bonding procedure without heat application was used. The total time at room temperature was below 48 h and therefore all devices are still in the state of beneficial annealing. Prior to bump bonding all sensors were characterized with IV-methods.

The bump bonded samples were tested at the CERN-SPS H2 beam line using 150 – 225 GeV pions. The pixel device under test was situated inbetween a four layer silicon strip telescope [8] with an effective spatial resolution of about $1 \mu\text{m}$. The whole set-up was placed in a 3 T magnet with the \vec{B} field parallel to the beam. The pixel detector was set either normal to the beam, or with a flat angle of 15° between the beam and the sensor surface. The measurements performed in magnetic field and under tilt are reported in ref. [9]. The irradiated sensors were operated at -20°C by the use of water cooled Peltier elements.

²PSI30 DMILL pixel readout chip was designed 1997 at Paul Scherrer Institut, Villigen, Switzerland, and translated 1998 to the Honeywell RICMOS IV process at 1. Physikalisches Institut of the RWTH Aachen, Germany.

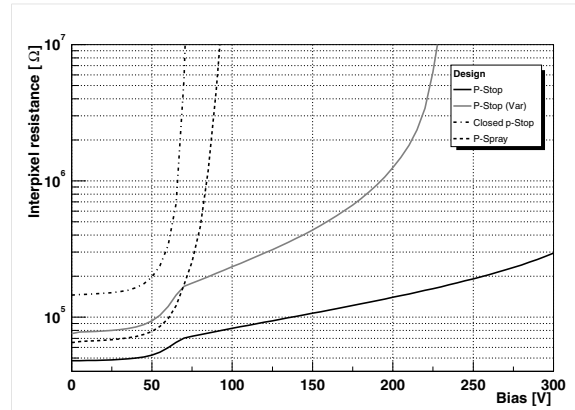


Fig. 2. Resistance between one pixel and all its neighbors as a function of the back side voltage. For comparison to the designs in fig. 1 (p -stop and p -spray) two other design options are also shown.

IV. RESULTS

A. Interpixel resistance

While p -spray isolated devices feature naturally high interpixel isolation the interpixel resistance of the p -stop devices depend very much on the geometry of the openings in the p -stops and the gap width.

Figure 2 shows the interpixel resistance of different pixel designs as a function of the sensor bias. An array of 5×5 pixels was grounded while the potential of the center pixel was elevated to $+1 \text{ V}$. The current flowing into this pixel was measured in dependence of the back side voltage. In order to illustrate the effect of the p -stop openings in the p -stop design shown in fig. 1 (left), an identical design with closed p -stops, a different p -stop geometry, and the p -spray option of fig. 1 (right) are also shown.

As the depletion starts from the back side (“ n -in- n ”), part of the current can pass via the bulk before full depletion is reached and therefore the interpixel resistance is low. When full depletion is reached this channel is pinched off and the resistance in the fully isolated devices increases rapidly by orders of magnitude. In the devices featuring p -stop openings a residual current flows over the electron accumulation layer. However, with the backside bias being increased further this electron channel also starts to be pinched off as visible in fig. 2 for the curve labeled p -stop (Var) at bias above 200 V.

The design called p -stop shows no pinch off up to 300 V. The interpixel resistance is only about 100 k Ω at a backside voltage of 150 V. This results in wide signal spreading along the resistive channels. The test beam data with the unirradiated device was therefore taken at 300 V bias where the interpixel resistance reaches a value of 300 k Ω and the signal spread is reduced.

For irradiated sensors the resistance of the electron accumulation layer is much higher (in the order of G Ω), more or less independent on the designs [2], [3].

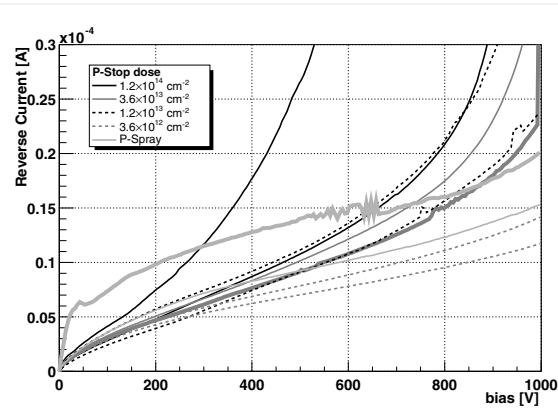


Fig. 3. IV curves of each two sensors (open p -stops, fig. 1, left) with different p -stop implantation doses irradiated to $\Phi = 8 \times 10^{14} \text{ n}_{\text{eq}}/\text{cm}^2$, measured at -20°C . For comparison two p -spray sensors (fig. 1, right) are also plotted. The devices used later in the test beam are plotted with bold lines.

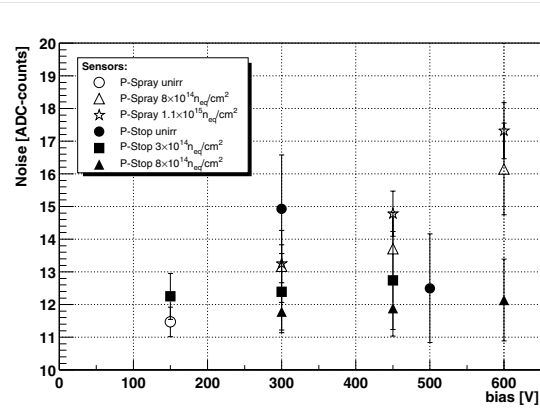


Fig. 4. Bias dependence of the noise in six bump bonded pixel sensors. The error bars indicate the variation (RMS) of noise over the sensor.

B. Characteristics and Noise

The current vs. voltage characteristic is a very sensitive tool to detect possible problems in a sensor. Especially after irradiation an early current increase is an indication for electrical breakdown. Early breakdown accompanied by noise increase was previously observed in irradiated p -stop isolated devices [3], [10] and is considered to be their major drawback.

To improve the breakdown behavior of the p -stop devices, implantation dose of the p -stop implant has systematically been reduced from the typically used 10^{14} cm^{-2} down to the p -spray level of $3 \times 10^{12} \text{ cm}^{-2}$. The IV-characteristics of these devices after a proton irradiation of $\Phi = 8 \times 10^{14} \text{ n}_{\text{eq}}/\text{cm}^2$ are plotted in fig. 3 together with two p -spray devices. It is visible that the current and the slope of the curve decreases with decreasing p -stop dose. The sensors with a p -stop dose of $3 \times 10^{12} \text{ cm}^{-2}$ show an IV-characteristic with has the same shape as the one of the p -spray sensors.

In total six sensors of the two designs have been bump bonded to readout chips. Since a full non zero-suppressed readout is possible, the noise of each pixel can be easily determined. In fig. 4 the bias dependence of the average pixel

noise is plotted for three sensors of each type irradiated to 0, 3, 8 and $11 \times 10^{14} \text{ n}_{\text{eq}}/\text{cm}^2$. 15 ADC-counts correspond to about 350 electrons noise. However this number represents only a rough estimation as an exact calibration was not yet performed.

For the two irradiated p -spray sensors we find a weak, uncritical noise increase from about 12 ADC counts at 300 V to 17 ADC counts at 600 V. The p -stop devices show a noise of about 12 ADC counts more or less independent on the bias voltage. The error bars in the fig. 4 represent the variation of the noise over the sensor (in terms of RMS). The fact that the width of the error bars does not show a significant increase, neither with bias nor with irradiation dose, indicates that there are no localized regions of high noise.

From the absence of noisy regions and from the shape of the IV-curves we conclude that electrical breakdown in p -stop isolated silicon detectors can be avoided by reducing the implantation dose to about 10^{13} cm^{-2} .

C. Charge Collection Properties

The high energy pion beam of the CERN SPS (150-225 GeV) together with the high precision beam telescope allows for a detailed resolution in the pixel detector under test with an accuracy of about $1 \mu\text{m}$. Of particular interest is the study of the charge collection efficiency as a function of the particle impact point in order to locate “blind” spots within every pixel.

Figure 5 displays the total cluster charge deposited by perpendicular tracks as function of the pixel impact position. The area shown represents one pixel cell with a pitch of $125 \mu\text{m}$ in both directions. The cluster signal was obtained by summing the signals of the 3×3 pixels around the impact point without threshold requirement. The average signal heights in the pixel center, in selected regions and averaged over the whole pixel area are given in table I.

For unirradiated p -spray sensors a very homogeneous signal height of about 810 ADC channels is observed. At the position of the bias dot the collected signal drops to about half of this value. As this critical area represents only 2–3 % of the total surface the average collected signal is hardly affected.

After irradiation at a fluence of $\Phi = 1 \times 10^{15} \text{ n}_{\text{eq}}/\text{cm}^2$ the value of total collected charge is reduced by almost 40 %. Furthermore an additional area of reduced charge collection appears at the metal line connecting the bias dots. As there is no direct contact between this metal line and the silicon below, this behavior (also reported in ref. [11]) is a priori unexpected and not yet fully understood. It seems plausible that the charge loss is caused by capacitive coupling. Before irradiation the metal line is shielded by the conductive p -spray layer. However after irradiation the p -spray layer behaves like a (bad) insulator and a charge drifting below this layer can induce an electrical signal on the bias line above.

Since the total affected area is under 10 %, the signal averaged over the whole pixel cell is about 5 % smaller than the signal collected in the central pixel region.

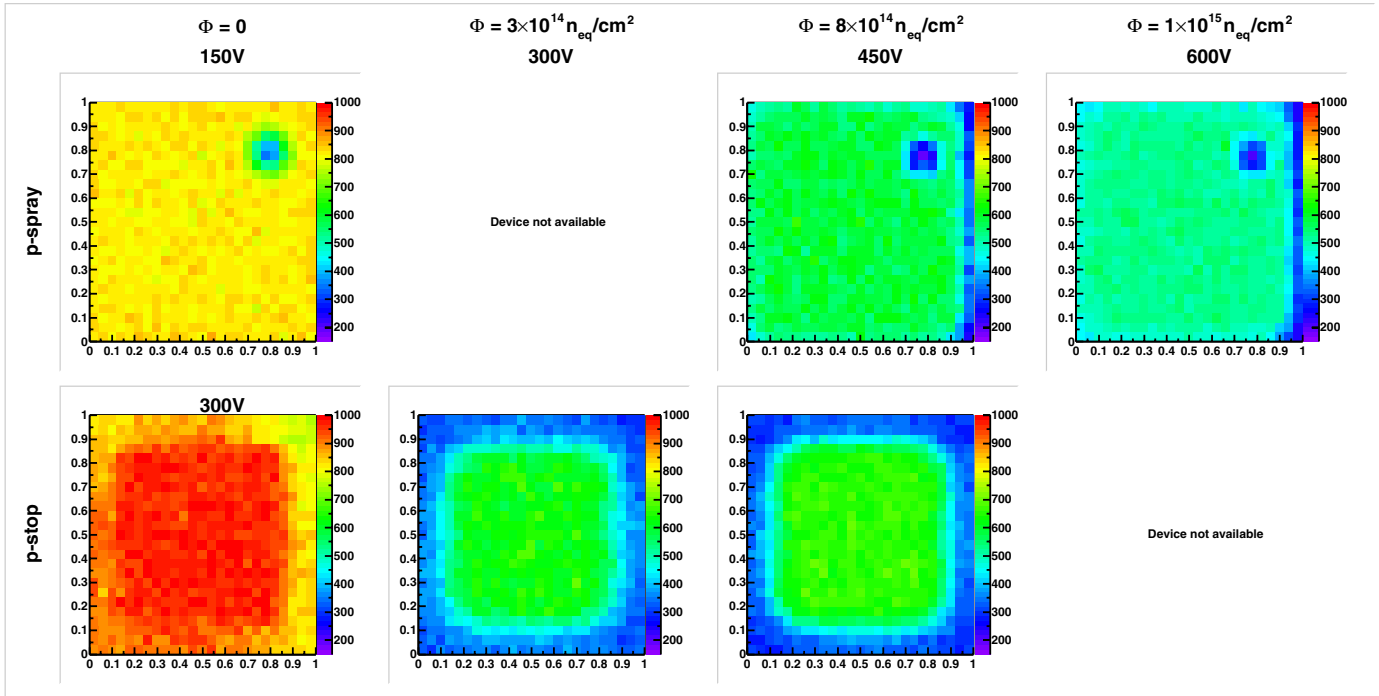


Fig. 5. Cluster charge collected in an area of 3×3 pixels in dependence of the point of incidence. The area shown represents one pixel cell of $125 \times 125 \mu\text{m}^2$, the charge is given in ADC counts. The p -spray (above) and the p -stop (below) design are shown.

Highest signals were observed on the unirradiated p -stop sensor, 950 ADC counts, about 15 % larger than the maximum in the p -spray devices. However, one has to take into account that a bias of 300 V was applied in order to suppress a charge spread due to resistive connections between pixels. The average cluster size for perpendicular tracks using a pixel threshold of 65 ADC counts is 3.1 compared to 1.3 for the p -spray design at 150 V.

Close to the pixel border the cluster signal decreases by about 13 % compared to the central region. For irradiated devices this signal drop in the border region becomes more pronounced. Only about 60 % of the signal is collected compared to a hit in the pixel center. Since the border region is quite large (see fig. 5), this leads to a heavy decrease of the average signal height. The reason for this significant charge loss is not fully understood but the following explanation seems reasonable: The electron accumulation layer between the p -stops adjusts to the same potential as the pixel implants due to the openings in the p -stops. For this reason the layer also collects charge. For the unirradiated sensor the surface mobility in the electron accumulation layer is high enough that the signal collected there is quickly transferred to the next readout n^+ -implant. In the irradiated sensors the mobility of free charge carriers close to the surface is strongly reduced and the number of surface traps increases. Therefore the charge drift to the next readout n^+ -implant is slower and a significant fraction of the signal might not reach it in time.

Φ [$n_{\text{eq}}/\text{cm}^2$]	Bias [V]	Mean Cluster Signal [ADC]			Efficiency at 65 ADC
		Average	Center	Border	
p -spray					
0	150	808	814	dot: 377	99.68 %
8×10^{14}	450	553	587	dot: < 260 line: 326	98.49 %
1.1×10^{15}	600	502	530	dot: < 300 line: 301	99.15 %
p -stop					
0	300	906	953	845	99.67 %
3×10^{14}	300	482	610	345	99.50 %
8×10^{14}	450	514	658	334	99.08 %

TABLE I

SUMMARY OF TEST BEAM RESULTS CONCERNING CHARGE COLLECTION PROPERTIES.

D. Efficiency

In the final operation of the pixel detector the important figure of merit is the probability for actually detecting a particle penetrating the detector. In order to translate the charge collection behavior discussed in the previous section into efficiency measures, thresholds have been required. If the pixel pointed to by the beam telescope or a direct neighbor was above the threshold, the track was counted as detected. A cluster threshold was not applied. Regions of defect bump bonding or noisy pixels were excluded from this analysis.

The choice of the threshold values is a bit arbitrary as the amplitude of the signal output has not yet been properly calibrated. A rough estimation from the analysis of tilted tracks indicates that 65 ADC channels correspond to a signal charge

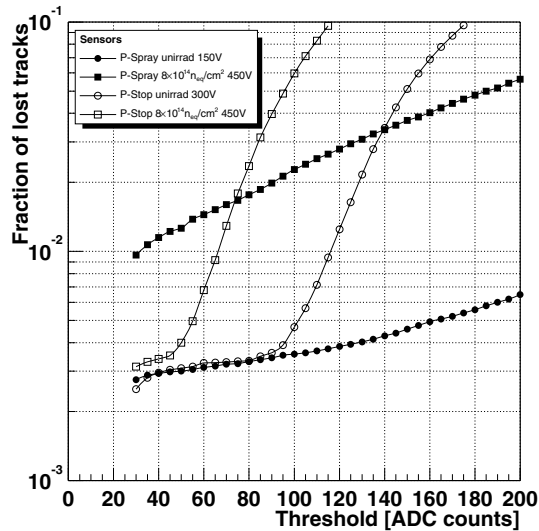


Fig. 6. Fraction of undetected tracks in the pixel detector as function of the applied threshold.

of about 2000 electrons. The probability for detecting a particle with a pixel threshold of 65 ADC channels is given in table I. In all cases it is above 98%.

The inefficiency as a function of the threshold is plotted in fig. 6 for both designs under study, and for proton fluences of 0 and $8 \times 10^{14} \text{ n}_{\text{eq}}/\text{cm}^2$. Here a difference between the designs is visible. In the unirradiated *p*-spray design the charge loss due to the bias dot is small enough not to cause an inefficiency if the pixel threshold is below 100 ADC counts. For higher thresholds the lost tracks start to concentrate around this area. In the case of the irradiated *p*-spray sensor the probability for losing a track hitting the bias dot is higher due to the lower total charge. Already at low threshold the total inefficiency is about 1%. With increasing threshold the inefficiency rises as also tracks hitting the region below the metal line of the bias grid start to contribute starting from the corner of the pixel and growing along the pixel edge below the metalization. When the threshold exceeds 130 ADC channels, a small accumulation of lost tracks can be found also in the corners opposite to the metal line. As the total problematic area is quite small, the slope of the increase is limited and the inefficiency does not exceed 4% even at high threshold (e.g. 160 ADC counts).

For the *p*-stop designs the situation looks different. As the charge loss in the pixel edge region is less drastic, the efficiency at low threshold is above 99.5% also for the irradiated sensor. However as the less efficient region at the pixel edge covers a significant fraction of the area, the inefficiency increases fast with increasing threshold. The lost tracks accumulate at the pixel corners. With increasing threshold the regions of lower efficiency grow along the pixel edges.

Although both sensor types reach a similar efficiency at a (quite realistic) threshold of 65 ADC counts, it has to be stressed that the high slope of the irradiated *p*-stop sensor

displays a potential risk as a small threshold variation can lead to a non tolerable inefficiency above 5%. The *p*-stop sensor has also been measured at a bias voltage of 600 V. The higher bias increases the collected charge and the detection efficiency, although not significantly.

V. CONCLUSIONS

Silicon pixel sensors of “*n*-in-*n*” type featuring *p*-spray and *p*-stop isolation have been irradiated to proton fluences up to $10^{15} \text{ n}_{\text{eq}}/\text{cm}^2$ and subsequently bump bonded to readout chips of the type PSI/AC30. This chip allows a non zero-suppressed analogue readout and is therefore well suited for sensor studies.

All sensors show IV-curves with a breakdown voltage well above 600 V without localized noisy regions. In the case of *p*-stop sensors this was achieved by reducing the *p*-stop implantation dose to about 10^{13} cm^{-2} .

The charge collection studies performed with high energy pions allowed a characterization of two different sensor designs. For *p*-spray sensors the bias dots represent an area with reduced charge collection. For irradiated devices the metal line of the bias grid also reduces charge collection. However tracks are detected with an efficiency exceeding 98% after an irradiation fluence of $8 \times 10^{14} \text{ n}_{\text{eq}}/\text{cm}^2$. The most inefficient region of the *p*-stop sensors is located in between the pixels. In unirradiated devices this leads to a particle detection efficiency exceeding 99.7%. However, especially in the irradiated device, this number drops dramatically for thresholds higher than 70 ADC counts. This steep increase of lost tracks seems to be the major drawback of this kind of device and has to be further investigated.

ACKNOWLEDGMENTS

The authors would like to thank Silvan Streuli from ETH Zürich and Fredy Glaus from PSI for their enormous effort in bump bonding, Maurice Glaser and Michael Moll from CERN for carrying out the irradiation, and Gyorgy Bencze and the CERN-SPS teams for their support during the test beam periods.

REFERENCES

- [1] The CMS Collaboration, *CMS Tracker Technical Design Report*, CERN/LHCC 98-6.
- [2] R. Kaufmann, *Development of radiation hard pixel sensors for the CMS experiment*. Dissertation der Universität Zürich, Zürich, 2001
- [3] G. Bolla et al., Nucl. Instr. and Meth. A 485 (2002) 89-99
- [4] G. Bolla et al., Nucl. Instr. and Meth. A 501 (2003) 160-163
- [5] G. Lindström et al., Nucl. Instr. and Meth. A 466 (2001) 308-326
- [6] T. Rohe et al., Nucl. Instr. and Meth. A 460 (2001) 55-66
- [7] D. Meer, *Bau und Messen eines Multichip Pixelmodules als Prototyp für den CMS-Tracker*, Diploma Thesis, ETH Zürich, March 2000
- [8] C. Amsler et al., Nucl. Instr. and Meth. A 480 (2002) 501-507
- [9] A. Dorokhov et al., *Test beam measurements on the silicon sensors of the CMS pixel detector*, presented at the 6th International Conference on Large Scale Applications and Radiation Hardness of Semiconductor Detectors, September 29-October 1, 2003 in Firenze, Italy, to be published in Nucl. Instr. and Meth. A.
- [10] D. Robinson et al. Nucl. Instr. and Meth. A 426 (1999) 28-33
- [11] T. Lari [ATLAS Pixel Collaboration], “Test beam results of ATLAS pixel sensors,” arXiv:hep-ex/0210045